# New Journal of Physics

The open access journal at the forefront of physics

CrossMark

PAPER

# Coherent quantum phase slip in two-component bosonic atomtronic circuits

A Gallemí[1,2], A Muñoz Mateo[1], R Mayol[1,2] and M Guilleumas[1,2]

[1] Departament d'Estructura i Constituents de la Matèria, Facultat de Física, Universitat de Barcelona, E-08028 Barcelona, Spain
[2] Institut de Nanociència i Nanotecnologia de la Universitat de Barcelona, IN²UB, E-08028 Barcelona, Spain

E-mail: gallemi@ecm.ub.edu

Keywords: phase slip, coherent coupling, flux qubit, toroidal geometry, spinor condensate

## Abstract

Coherent quantum phase slip consists in the coherent transfer of vortices in superfluids. We investigate this phenomenon in two miscible coherently coupled components of a spinor Bose gas confined in a toroidal trap. After imprinting different vortex states, i.e. states with quantized circulation, on each component, we demonstrate that during the whole dynamics the system remains in a linear superposition of two current states in spite of the nonlinearity, and can be mapped onto a linear Josephson problem. We propose this system as a good candidate for the realization of a Mooij–Harmans qubit and remark its feasibility for implementation in current experiments with $^{87}$Rb, since we have used values for the physical parameters currently available in laboratories.

## 1. Introduction

The possibility to set up experiments devoted to the testing of quantum phenomena has been the subject of increasing interest since the discovery of superconductivity. At an early stage, this research led to the realization of superconducting quantum interference devices (SQUIDs) [1, 2]. Three decades later, the achievement of ultracold degenerate quantum gases, like Bose–Einstein condensates (BECs) [3, 4], opened up new opportunities to test quantum interference phenomena and their implementation in atomtronic quantum interference devices (AQUIDs) [5–10], the atomic analogue of SQUIDs. This duality between superfluid atomic gases and superconductors has made both systems stand out as good supports for quantum simulation. However, the tunability of the interaction and the versatility of atoms in simulating both bosonic and fermionic systems, provide a more promising perspective for the implementation of AQUIDs in future technological applications.

Josephson junctions play a key role in the physics of quantum interference devices. They constitute two quantum systems connected by a weak link, and can be classified in two categories (short and long), owing to the different nature of the coupling. In a short Josephson junction, the coherent transfer of physical quantities occurs through a single point, the Josephson link [11, 12]. When the junction is long, the coupling occurs locally at each point of the connection. In particular, two spin components of a condensate coupled by a Raman laser operate as a long Josephson junction, which is referred to in the literature as the internal Josephson effect [13], and obeys the Josephson equations with a coupling proportional to the overlap between condensates [14]. These techniques, by selecting an appropriate spatial dependence of the coupling, led to the first observation of vortices in BECs [15, 16].

Anderson [17] discussed the role of the phase of the order parameter in superfluids, which motivated the study of phase slips in superconductivity [18], liquid helium [19], and BECs [8, 10]. A phase slip event is a sudden change of the phase in $2\pi$ due to the motion of quantized vortices through a superfluid. This phenomenon is associated to dissipation, as pointed out by Langer and Ambegaokar [20]. Ultracold atoms, as superfluids, can also exhibit phase slips, by winding the phase through solitonic states [21–25], and they are able to generate quantum superpositions of macroscopic flows [26]. The literature includes several proposals to engineer superpositions of flow states in 1D quantum gases in continuous rings [27, 28] and discrete rings [31–35] (toroidal condensates in the presence of a lattice potential in the tight-binding regime [29, 30]).

Coherent quantum phase slip (CQPS) is an effect recently discovered in superconducting systems containing loops [36]. It is the dual phenomenon of the Josephson effect, which is a coherent transport of particles between two superfluids, but, in contrast, CQPS is defined as the coherent transfer of vortices through the Josephson link. In CQPS, the stationary states corresponding to flux quanta states become coupled, such that one can continuously change the flux quanta of the system. The Mooij–Harmans qubit [37, 38], which consists of a superconducting loop with a weak nanowire, was predicted to be able to manifest CQPS between two current states. The proposal was made a reality in the experiment of [36], which led to the first experimental observation of CQPS.

In this work, in order to generate CQPS, we propose the realization of an atomic analogue of the Mooij–Harmans qubit by means of a spinor condensate with two relevant internal degrees of freedom or spin states. The two components are coupled by phase (spin exchange) and density (contact interaction), and both occupy the same space region, since the interspecies density repulsion is small enough to keep the system in the miscible phase. Therefore, this overlap allows the coupling to occur locally, point to point, in the whole bulk of the condensate (long Josephson junction). With the aim of engineering a qubit we will select vortex states as the basis of an effective two-level system that is able to perform qubit operations [39]. The coherent coupling transfers vortices between both components in the absence of population imbalance, and the nonlinear system exhibits Rabi oscillations. We consider condensates confined in ring geometries, where persistent currents are metastable states and phase slips provide the mechanism for the system to exchange winding numbers between components. All these properties make the system stand out as a promising tool for atomtronic circuits, and in particular, for the simulation of CQPS.

The paper is organized as follows. In section 2, we present the mean field model we have used to study the system of two miscible coherently coupled condensates. Section 3 characterizes the different dynamical regimes that the system exhibits as a function of the coherent coupling and interaction. In section 4 we discuss the regime where the system shows CQPS and propose an analytical model that accurately reproduces our numerical results. Section 5 is devoted to the other dynamical regimes of the phase diagram, and finally, section 6 summarizes our work and provides future perspectives.

## 2. Theoretical framework

To describe the system of two coherently coupled Bose–Einstein condensates in the mean field regime, we will use the Gross–Pitaevskii equation (GPE) for the wavefunctions $\Psi_\uparrow$ and $\Psi_\downarrow$:

$$i\hbar\frac{\partial}{\partial t}\Psi_\uparrow = \mathcal{H}_0\Psi_\uparrow + g_{\uparrow\uparrow}|\Psi_\uparrow|^2\Psi_\uparrow + g_{\uparrow\downarrow}|\Psi_\downarrow|^2\Psi_\uparrow + \frac{\hbar\Omega}{2}\Psi_\downarrow$$

$$i\hbar\frac{\partial}{\partial t}\Psi_\downarrow = \mathcal{H}_0\Psi_\downarrow + g_{\downarrow\downarrow}|\Psi_\downarrow|^2\Psi_\downarrow + g_{\uparrow\downarrow}|\Psi_\uparrow|^2\Psi_\downarrow + \frac{\hbar\Omega}{2}\Psi_\uparrow, \tag{1}$$
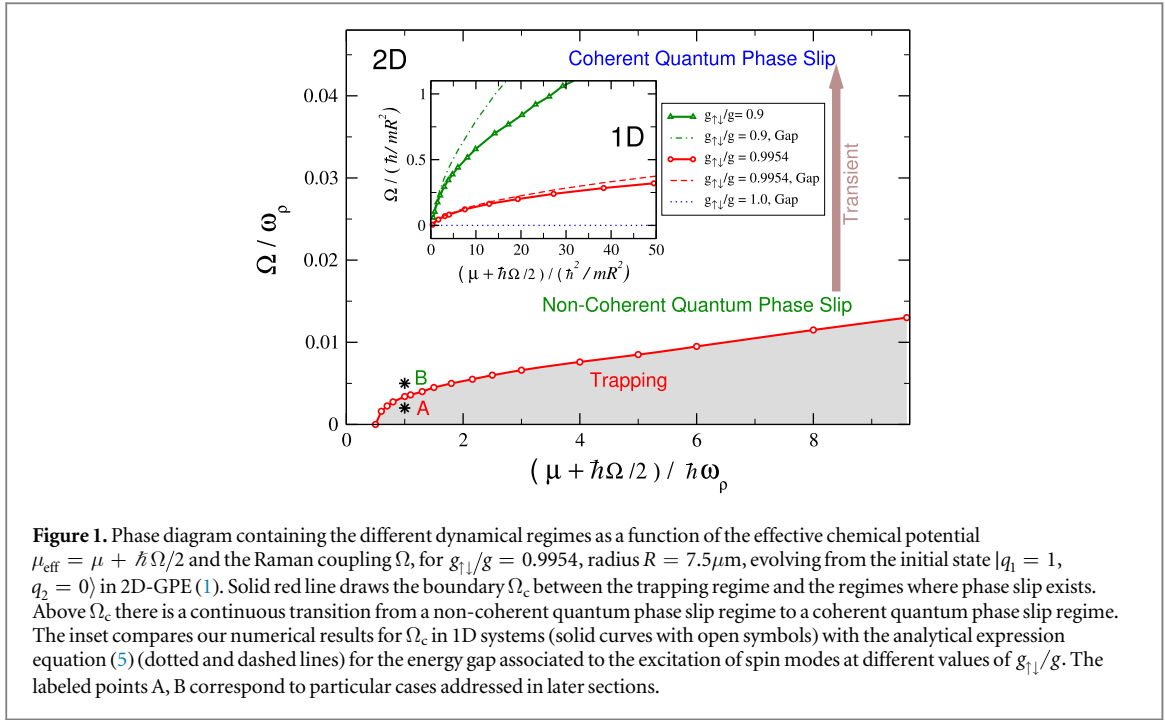
where $\mathcal{H}_0 = -\hbar^2/2m\,\vec{\nabla}^2 + V_{\mathrm{trap}}$, $g_i = 4\pi\hbar^2 a_i/m$, with $i = \uparrow\uparrow, \downarrow\downarrow, \uparrow\downarrow$, is the interaction strength, $a_i$ is the scattering length, and the angular frequency $\Omega$ is the coherent Raman coupling that forces the two components to share the chemical potential $\mu$. We will consider multiply connected geometries by using a toroidal trap of radius $R$, $V_{\mathrm{trap}} = 1/2m\,\omega_\rho^2((\rho - R)^2 + \lambda^2 z^2)$, with angular frequency $\omega_\rho$, and aspect ratio $\lambda \gg 1$. For quasi-2D systems the interaction strength takes the value $\sqrt{\hbar/m\,\omega_z}\,g_i^{2D}/g_i = 1/\sqrt{2\pi}$.

The time-independent solutions $\Psi(\vec{r}, t) = \phi(\vec{r})\exp(-i\mu t/\hbar)$ of equation (1) can be found by solving:

$$\mu\phi_\uparrow = \mathcal{H}_0\phi_\uparrow + g_{\uparrow\uparrow}\left|\phi_\uparrow\right|^2\phi_\uparrow + g_{\uparrow\downarrow}|\phi_\downarrow|^2\phi_\uparrow + \frac{\Omega}{2}\phi_\downarrow$$

$$\mu\phi_\downarrow = \mathcal{H}_0\phi_\downarrow + g_{\downarrow\downarrow}\left|\phi_\downarrow\right|^2\phi_\downarrow + g_{\uparrow\downarrow}|\phi_\uparrow|^2\phi_\downarrow + \frac{\Omega}{2}\phi_\uparrow, \tag{2}$$

where all the quantities are written in terms of the harmonic oscillator units, by using $\hbar\,\omega_\rho$ and $\sqrt{\hbar/m\,\omega_\rho}$ as energy and length units, respectively. In our simulation we also consider $g_{\uparrow\uparrow} = g_{\downarrow\downarrow} = g \gtrsim g_{\uparrow\downarrow}$ to ensure miscibility. The total number of particles $N$ is fixed, in such a way that $\sum_i \int \phi_i^*(\vec{r})\phi_i(\vec{r})\,d\vec{r} = N$, though particles of both components can exchange their spin by virtue of the coherent Raman coupling.

Analytical expressions can be obtained within the Thomas–Fermi approach in order to study the ground state properties of the condensate in the regime of large interactions. In the case without Raman coupling [40–42], the Thomas–Fermi wavefunction is the same for both components: $\psi^{\mathrm{TF}} = \sqrt{(\mu - V_{\mathrm{trap}})/(g + g_{\uparrow\downarrow})}$. Such expression will be also useful in the presence of Raman coupling, where the ground state satisfies $\psi_\uparrow = -\psi_\downarrow$ for $\Omega > 0$ [43], since a phase difference of $\pi$ between both components minimizes the mean field energy. Therefore, the Raman coupling $\Omega$ becomes a simple shift of the chemical potential and the Thomas–Fermi wavefunctions can be written as

**Figure 1.** Phase diagram containing the different dynamical regimes as a function of the effective chemical potential $\mu_{\text{eff}} = \mu + \hbar\Omega/2$ and the Raman coupling $\Omega$, for $g_{\uparrow\downarrow}/g = 0.9954$, radius $R = 7.5\,\mu$m, evolving from the initial state $|q_1 = 1$, $q_2 = 0\rangle$ in 2D-GPE (1). Solid red line draws the boundary $\Omega_c$ between the trapping regime and the regimes where phase slip exists. Above $\Omega_c$ there is a continuous transition from a non-coherent quantum phase slip regime to a coherent quantum phase slip regime. The inset compares our numerical results for $\Omega_c$ in 1D systems (solid curves with open symbols) with the analytical expression equation (5) (dotted and dashed lines) for the energy gap associated to the excitation of spin modes at different values of $g_{\uparrow\downarrow}/g$. The labeled points A, B correspond to particular cases addressed in later sections.

$$\psi_\uparrow^{\text{TF}} = -\psi_\downarrow^{\text{TF}} = \sqrt{\frac{\mu_{\text{eff}} - V_{\text{trap}}}{g + g_{\uparrow\downarrow}}}, \tag{3}$$

where $\mu_{\text{eff}} = \mu + \Omega/2$ will play the role of an effective chemical potential for the coupled system.

We will also explore the effect of vortices on stationary states. Their associated angular momentum per particle is $\hbar q$ for each component, where $q$ is the winding number or charge of the vortex, when it is centered. This is no longer true for off-centered vortices. Nevertheless, one can give an expression for the dependence of the angular momentum as a function of the position $r_i$ of the off-centered vortex, by following the procedure developed in [44, 45] for the case of a condensate in a harmonic trap in the Thomas–Fermi limit, since in this regime, the effect of the vortex on the density profile can be neglected. We have derived the expression for the contribution on the angular momentum per particle of a vortex in the density region of a 2D ring:

$$\frac{L_z^i}{N\hbar q} = \frac{3}{32}\frac{\delta}{R}\left(1 - \eta^2\right)^2 - \frac{\eta}{8}\left(3 - \eta^2\right) + 1, \tag{4}$$

where $\eta = (r_i - R)/\delta$ and $R \pm \delta$ are the external and internal Thomas–Fermi radius, respectively, and $\delta = \sqrt{2\mu} = [3(a + a_{\uparrow\downarrow})N/2R]^{1/3}$ is the half-width of the torus in harmonic oscillator units.

## 3. Dynamical regimes of two coupled condensates in a ring

We investigate the transfer of vortices between two coherently coupled BECs by solving numerically the time dependent GPE (1). To this aim, we have selected typical experimental values of the physical parameters. We first compute the ground state of a two-component $^{87}$Rb spinor condensate with intraspecies scattering length $a = 101.41\,a_{\text{B}}$ and $a_{\uparrow\downarrow} = 100.94\,a_{\text{B}}$, where $a_{\text{B}}$ is the Bohr radius, corresponding to the hyperfine states $|F = 1, m_F = 0\rangle$ and $|F = 1, m_F = -1\rangle$. The system is confined in a toroidal trap, with frequency $\omega_\rho = 2\pi \times 200$ Hz, aspect ratio $\lambda = 4$, and radius $R = 7.5\,\mu$m. Afterwards, persistent currents are induced in each component, with different winding numbers $q_\uparrow$ and $q_\downarrow$, by imprinting proper phases, i.e. $\Psi_i \to \Psi_i \times \exp(iq_i\theta)$, and the system, whose state will be described by the pair $|q_\uparrow, q_\downarrow\rangle$, is allowed to evolve.

In figure 1 we show the dynamical regimes of the system, for the initial state $|q_1 = 1, q_2 = 0\rangle$, obtained by numerical simulations of equation (1). Depending on the values of the effective chemical potential and the Raman coupling, the system explores three different regimes that will be explained in detail in the following sections [46]. For values of the Raman coupling smaller than a critical one $\Omega_c$ (solid lines) we have found a vortex trapping regime, where winding number states can not be exchanged between components. We have also explored the influence of the ratio $g_{\uparrow\downarrow}/g$ by performing 1D numerical calculations of the spinor GPE, which are shown by solid lines and open symbols in the inset of figure 1. Open circles correspond to our results for $g_{\uparrow\downarrow}/g = 0.9954$, whereas triangles correspond to $g_{\uparrow\downarrow}/g = 0.9$.

It has been demonstrated that in order to produce spin excitations [47, 48], which are the relevant ones for phase slips in a spinor condensate, it is necessary to overcome an energy gap $\Delta$ given by:

$$\Delta = \Omega \sqrt{1 + \frac{ng}{\Omega}\left(1 - \frac{g_{\uparrow\downarrow}}{g}\right)}, \tag{5}$$

where $n$ is the total density. For the sake of comparison, we have complemented the inset of figure 1 with the curves given by equation (5) for the same numerical values of $\Omega_c$: dotted ($g_{\uparrow\downarrow}/g = 1.0$), dashed ($g_{\uparrow\downarrow}/g = 0.9954$) and dotted–dashed ($g_{\uparrow\downarrow}/g = 0.9$) lines. The minimal coupling energy $\hbar\Omega_c$ necessary to produce phase slip is of the order of $\Delta$. When $g_{\uparrow\downarrow} = g$, phase slips can be produced for arbitrarily small values of the coherent coupling. As the ratio $g_{\uparrow\downarrow}/g$ decreases the energy cost for producing phase slips increases.

Once this gap is overcome, phase slip is possible. The system continuously transits from the non-coherent quantum phase slip (NCQPS) regime at $\Omega \gtrsim \Omega_c$, where vortex exchange between components can be observed at rates different from $\Omega$, to the CQPS regime at $\Omega \gg \Omega_c$. We identify a process as coherent if phase slip events occur with a complete transfer of angular momentum between the components and with a frequency of oscillation equal to the Raman coupling, together with the fact that only two vortex states are involved in the dynamics. If phase slip events occur without following the previous description, we classify the regime as non-coherent.

The dynamical phase diagram also depends on the radius of the torus. As the ring geometry constitutes a finite system, a zero-point kinetic energy $\hbar^2/mR^2$ is introduced. This energy quantum separates winding number states and, as a result, the degenerate states $|q_1, q_2\rangle$ and $|q_2, q_1\rangle$ are separated by a gap from other winding number states. When the radius of the torus increases, the zero-point kinetic energy goes to zero and the energy spectrum becomes a continuum. The same occurs when the interaction energy is very large, because the energy to produce a vortex is negligible in front of the chemical potential. As we will show later, CQPS decays or is even absent in these cases. The dynamical phase diagram can also exhibit dramatic changes in the immiscible case, where vortex states can split due to phase separation [49].

## 4. Coherent quantum phase slip

In order to have an analytical insight into the dynamics of the system, one can follow the spirit of the two-mode approximation. In the CQPS regime, the condensate wavefunction can be written as [16, 50, 51]:

$$\begin{pmatrix} \Psi_{\uparrow}(\vec{r}, t) \\ \Psi_{\downarrow}(\vec{r}, t) \end{pmatrix} = \phi_{q_1}(\vec{r})\begin{pmatrix} \psi_{\uparrow,q_1}(t) \\ \psi_{\downarrow,q_1}(t) \end{pmatrix} + \phi_{q_2}(\vec{r})\begin{pmatrix} \psi_{\uparrow,q_2}(t) \\ \psi_{\downarrow,q_2}(t) \end{pmatrix}, \tag{6}$$

where $\phi_{q_j}(\vec{r}) = \phi_{q_j}(\rho) \times e^{iq_j\theta}$, with $j = 1, 2$, are eigenvectors of both the angular momentum operator $\hat{L}_z$, with eigenvalue $\hbar q_j$, and the Hamiltonian without Raman coupling, with eigenvalue $\mu_j$. This ansatz neglects any contribution from other modes with charges different from $q_1$ and $q_2$. As we will see later, our numerical results agree with this assumption, since the only eigenvectors that significantly contribute to the dynamics are those associated to the winding numbers imprinted initially onto the wavefunction.
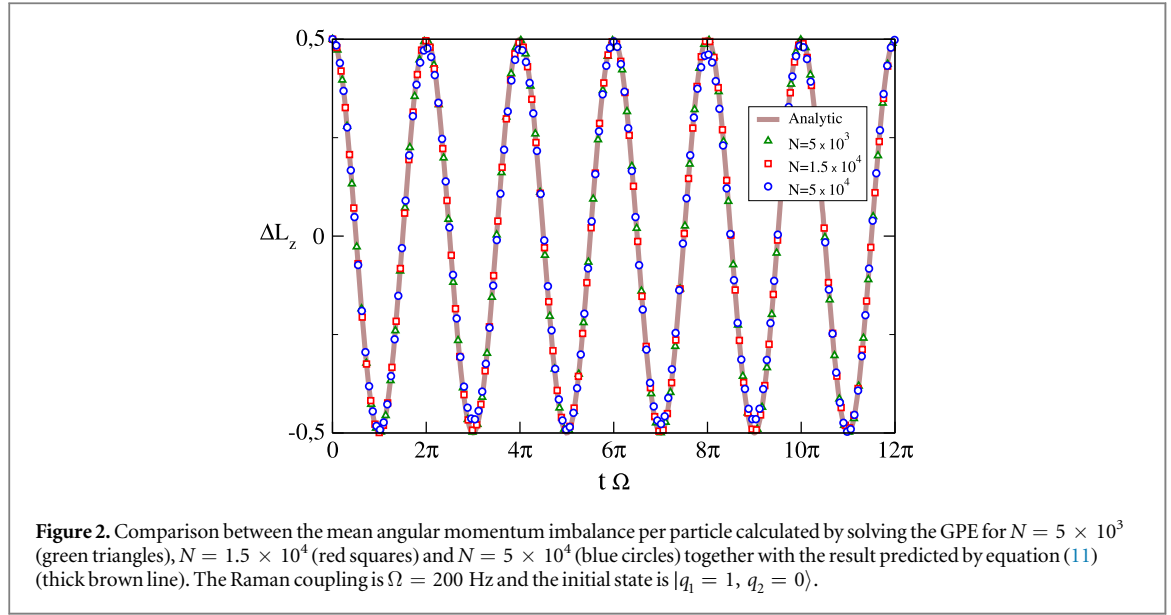
After substituting equation (6) in the GPE (1) one gets two decoupled linear Josephson equations for each winding number:

$$\begin{aligned} i\hbar\frac{\partial \psi_{\uparrow,q_1}}{\partial t} &= \mu_1 \psi_{\uparrow,q_1} + \frac{\hbar\Omega}{2}\psi_{\downarrow,q_1} \\ i\hbar\frac{\partial \psi_{\downarrow,q_1}}{\partial t} &= \mu_1 \psi_{\downarrow,q_1} + \frac{\hbar\Omega}{2}\psi_{\uparrow,q_1}, \end{aligned} \tag{7}$$

and

$$\begin{aligned} i\hbar\frac{\partial \psi_{\uparrow,q_2}}{\partial t} &= \mu_2 \psi_{\uparrow,q_2} + \frac{\hbar\Omega}{2}\psi_{\downarrow,q_2} \\ i\hbar\frac{\partial \psi_{\downarrow,q_2}}{\partial t} &= \mu_2 \psi_{\downarrow,q_2} + \frac{\hbar\Omega}{2}\psi_{\uparrow,q_2}. \end{aligned} \tag{8}$$

The straightforward solution of these linear systems has the eigenvalues $\mu_j \pm \Omega/2$. The energy gap between the two levels is $\Omega$, which is the driving frequency, then the solution for the condensate wavefunction is:

**Figure 2.** Comparison between the mean angular momentum imbalance per particle calculated by solving the GPE for $N = 5 \times 10^3$ (green triangles), $N = 1.5 \times 10^4$ (red squares) and $N = 5 \times 10^4$ (blue circles) together with the result predicted by equation (11) (thick brown line). The Raman coupling is $\Omega = 200$ Hz and the initial state is $|q_1 = 1, q_2 = 0\rangle$.

$$
\begin{pmatrix} \Psi_\uparrow(\vec{r}, t) \\ \Psi_\downarrow(\vec{r}, t) \end{pmatrix} = \phi_{q_1}(\rho)\, \mathrm{e}^{-\mathrm{i}\left(\mu_1 t/\hbar - q_1 \theta\right)} \begin{pmatrix} \cos\dfrac{\Omega t}{2} \\ -\mathrm{i}\sin\dfrac{\Omega t}{2} \end{pmatrix} + \phi_{q_2}(\rho)\, \mathrm{e}^{-\mathrm{i}\left(\mu_2 t/\hbar - q_2 \theta + \varphi\right)} \begin{pmatrix} -\mathrm{i}\sin\dfrac{\Omega t}{2} \\ \cos\dfrac{\Omega t}{2} \end{pmatrix},
\tag{9}
$$

and the corresponding densities read:

$$
\begin{aligned}
|\Psi_i|^2 = \frac{1}{2} \Big\{ &|\phi_{q_1}|^2 \cos^2\left(\frac{\Omega t}{2}\right) + |\phi_{q_2}|^2 \sin^2\left(\frac{\Omega t}{2}\right) \\
&\pm |\phi_{q_1}||\phi_{q_2}| \sin(\Omega t)\sin\left(\Delta\mu_q t/\hbar - \Delta q\,\theta + \varphi\right) \Big\},
\end{aligned}
\tag{10}
$$

where $\Delta q = q_2 - q_1$ is the initial winding number imbalance, $\Delta\mu_q = \mu_2 - \mu_1$ is the associated chemical potential imbalance, and $\varphi$ is an arbitrary phase.

From equation (9) one can get the mean angular momentum imbalance per particle $\Delta L_z = (\langle\Psi_\uparrow|L_z|\Psi_\uparrow\rangle - \langle\Psi_\downarrow|L_z|\Psi_\downarrow\rangle)/\hbar N$, as a function of time:

$$
\Delta L_z = \frac{\Delta q}{2}\cos(\Omega t).
\tag{11}
$$

This expression predicts that the exchange of vortices oscillates with the coherent coupling frequency $\Omega$. As a consequence, a $\pi$-pulse exchanges the winding numbers between components, and a $\pi/2$-pulse will drive each component to a quantum superposition of flows with winding numbers $q_1$ and $q_2$.
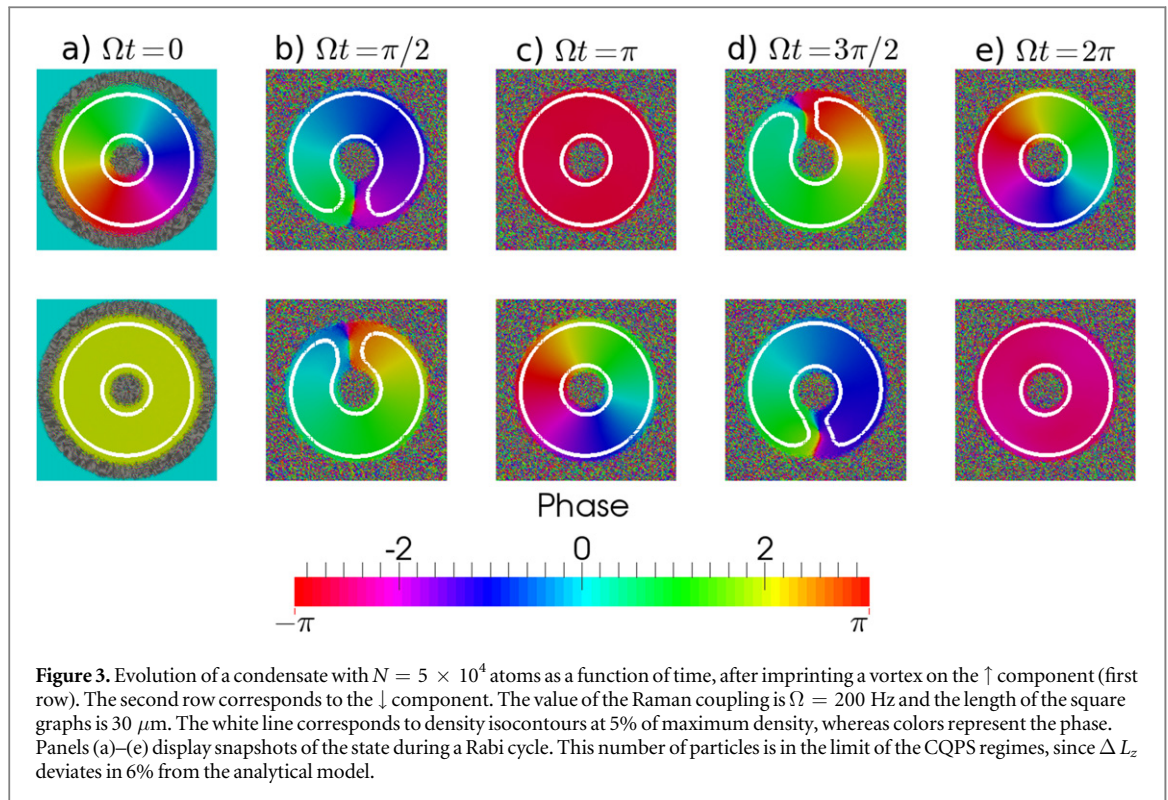
### 4.1. Phase slip between adjacent winding numbers

Figure 2 shows our numerical results, within the CQPS regime, for the mean angular momentum imbalance per particle, obtained by solving the GPE (1) in condensates with different number of particles and $\Omega = 0.16\,\omega_\rho$ (which corresponds to 200 Hz). The comparison with the analytical prediction given by equation (11) is also shown. As can be seen, the agreement is very good. The frequency of the oscillation of $\Delta L_z$ is precisely the Raman coupling $\Omega$ that coherently connects both spin components. The population imbalance is initially zero, and remains unaltered during the whole simulation, thus one can deduce that the spin exchange occurs 'at pairs' even though the population of both spin components is not fixed. By 'at pairs' we mean that for each particle of one condensate component flipping its spin there exists another particle of the other component doing the same.

In order to elucidate how the topological structure of the wavefunction changes as a function of time, we show in figure 3 the dynamical evolution of the density and the local phase for a condensate with $N = 5 \times 10^4$ atoms. White lines represent density isocontours at 5% of maximum density and colors depict the phase. Initially, at $t = 0$, we have imprinted a persistent current ($q_1 = 1$) in the $\uparrow$ component while the other is at rest (panel (a)). A quarter of period later, $\Omega t = \pi/2$, an azimuthal density node[3] is formed spontaneously in each component, at opposite positions (panel (b)). The vortex that was inducing the rotation in the initial state

---

[3] This objects should not be confused with dark solitons, since they can also appear in the linear case and the associated healing length is, in general, much larger than the one of solitary waves.

**Figure 3.** Evolution of a condensate with $N = 5 \times 10^4$ atoms as a function of time, after imprinting a vortex on the ↑ component (first row). The second row corresponds to the ↓ component. The value of the Raman coupling is $\Omega = 200$ Hz and the length of the square graphs is 30 $\mu$m. The white line corresponds to density isocontours at 5% of maximum density, whereas colors represent the phase. Panels (a)–(e) display snapshots of the state during a Rabi cycle. This number of particles is in the limit of the CQPS regimes, since $\Delta L_z$ deviates in 6% from the analytical model.

escapes from the ↑ component through the density depletion, while another vortex crosses the corresponding node in the ↓ component, transferring vorticity from the ↑ component to the ↓ component (panel (c)). This is the mechanism followed by the coupled system to produce $2\pi$-phase slips. After that, in panel (d) the evolution is reversed, returning the vorticity to the ↑ component (panel (e)), and so on.
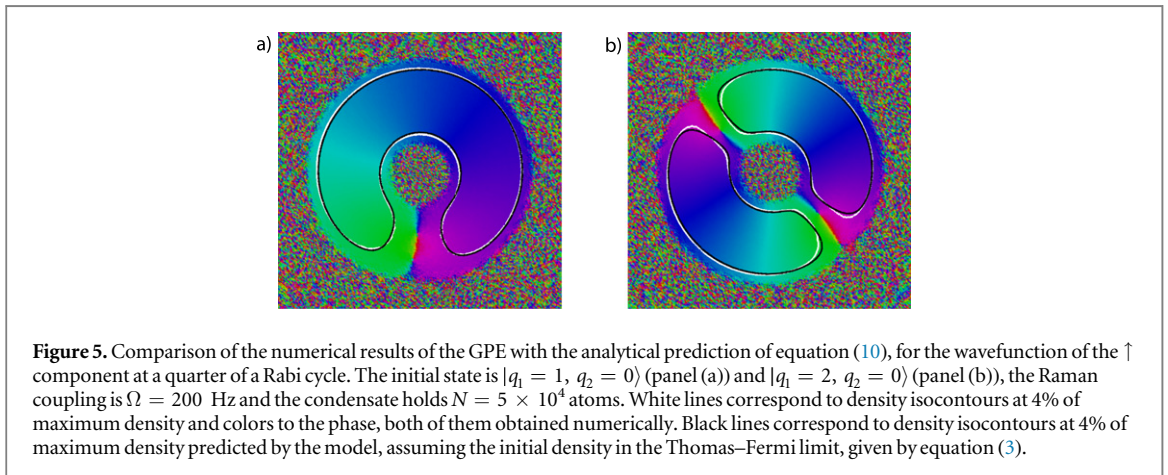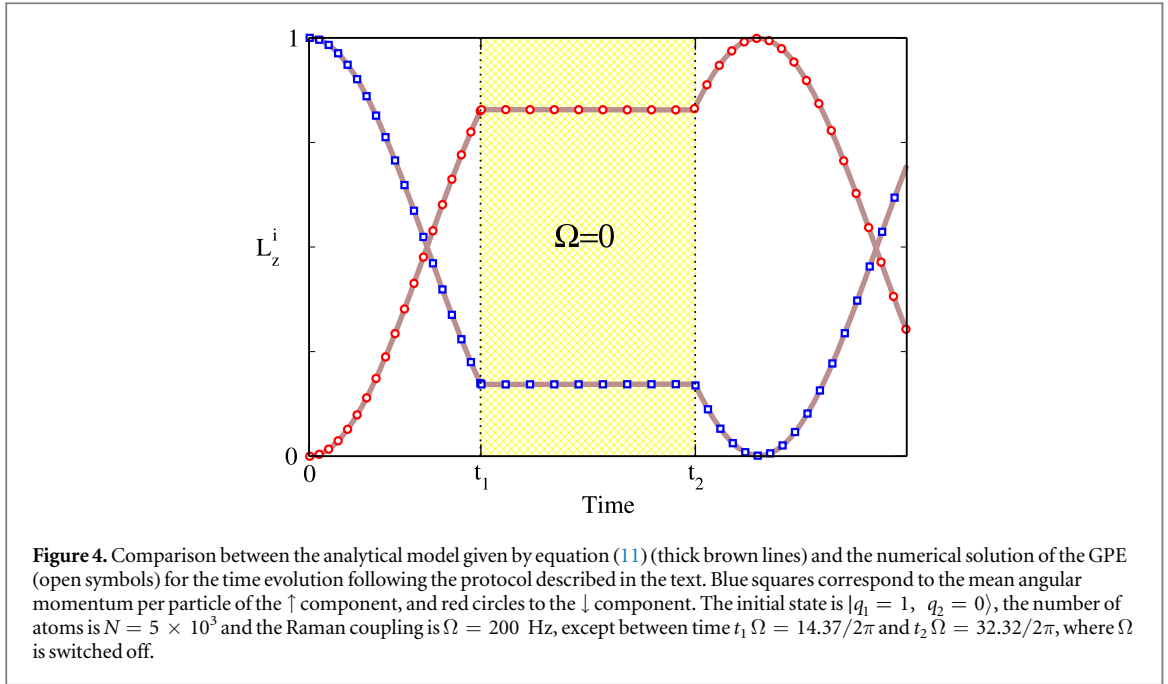
　　　CQPS in atomtronic circuits allows the system to effectively operate as a qubit. A quantum mechanical system is a good candidate for qubit manipulation if two conditions are fulfilled. First, the system must be considered as an effective two-state system, and second, at every time, the qubit must be expressed in a quantum superposition of both states. In our system these two states are $|q_1, q_2\rangle$ and $|q_2, q_1\rangle$, and as a result the state of the system can be written as $\Psi = \alpha |q_1, q_2\rangle + e^{i\gamma}\beta |q_2, q_1\rangle$ at every time, where $\alpha = \cos(\Omega t/2)$, $\beta = \sin(\Omega t/2)$, and $\gamma = -\pi/2$. The mapping is characterized by a periodic evolution with a period of $2\pi/\Omega$. At half a period, the phases of both components are exchanged, and in between, topological defects appear in the wavefunction in order to drive the phase slip. The Raman coupling $\Omega$ is a parameter that can be externally manipulated, and its control allows to simulate a tunable single-qubit quantum gate for quantum information processes. In this regime, the system displays two characteristic properties.

- The system behaves as linear despite the nonlinearity, since the Rabi frequency is the Raman coupling, independently of the interaction.

- The evolution occurs following quasi-stationary states.

　　　The two previous remarkable properties can be demonstrated by following this protocol: (a) evolve the system with a certain value of $\Omega$ in the CQPS regime, thus the angular momentum imbalance will oscillate with frequency $\Omega$. (b) At an arbitrary time $t_1$, switch the Raman coupling to zero, suppressing the exchange of phase between components. (c) At another arbitrary time $t_2$, switch on again the Raman coupling to its initial value in the process. Figure 4 represents the whole sequence of this protocol. At $t_1$ the state gets frozen in a quasi-stationary state rotating at a given velocity according to the winding number chemical potential imbalance. Then, at $t_2$ the evolution resumes, with exactly the same properties of the system at $t_1$. The curves predicted by the analytical model accurately fit in with the solution of the GPE.

### 4.2. Phase slip between non-adjacent winding numbers

All the results presented in section 4.1 are devoted to the case of CQPS between adjacent winding number states. However, the analytical model is more generic and also applies between non-adjacent winding numbers. In this

**Figure 4.** Comparison between the analytical model given by equation (11) (thick brown lines) and the numerical solution of the GPE (open symbols) for the time evolution following the protocol described in the text. Blue squares correspond to the mean angular momentum per particle of the ↑ component, and red circles to the ↓ component. The initial state is $|q_1 = 1, \; q_2 = 0\rangle$, the number of atoms is $N = 5 \times 10^3$ and the Raman coupling is $\Omega = 200$ Hz, except between time $t_1 \Omega = 14.37/2\pi$ and $t_2 \Omega = 32.32/2\pi$, where $\Omega$ is switched off.



**Figure 5.** Comparison of the numerical results of the GPE with the analytical prediction of equation (10), for the wavefunction of the ↑ component at a quarter of a Rabi cycle. The initial state is $|q_1 = 1, \; q_2 = 0\rangle$ (panel (a)) and $|q_1 = 2, \; q_2 = 0\rangle$ (panel (b)), the Raman coupling is $\Omega = 200$ Hz and the condensate holds $N = 5 \times 10^4$ atoms. White lines correspond to density isocontours at 4% of maximum density and colors to the phase, both of them obtained numerically. Black lines correspond to density isocontours at 4% of maximum density predicted by the model, assuming the initial density in the Thomas–Fermi limit, given by equation (3).
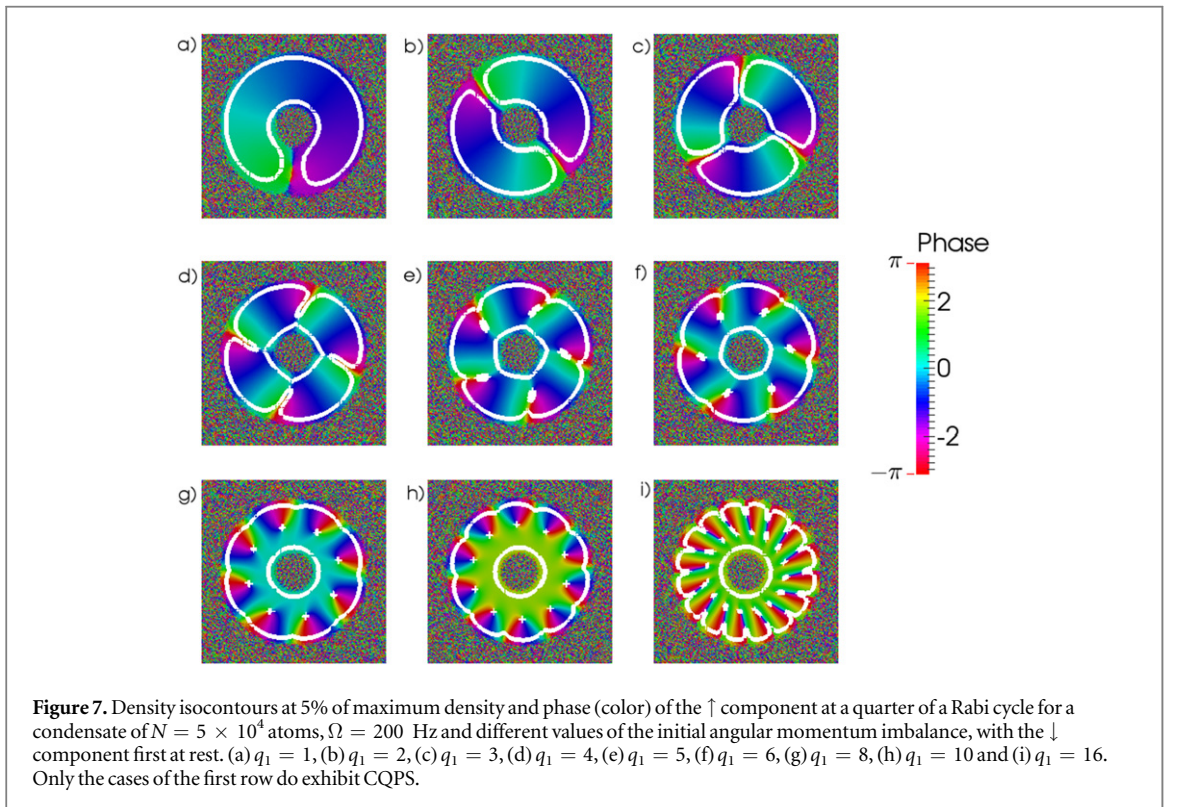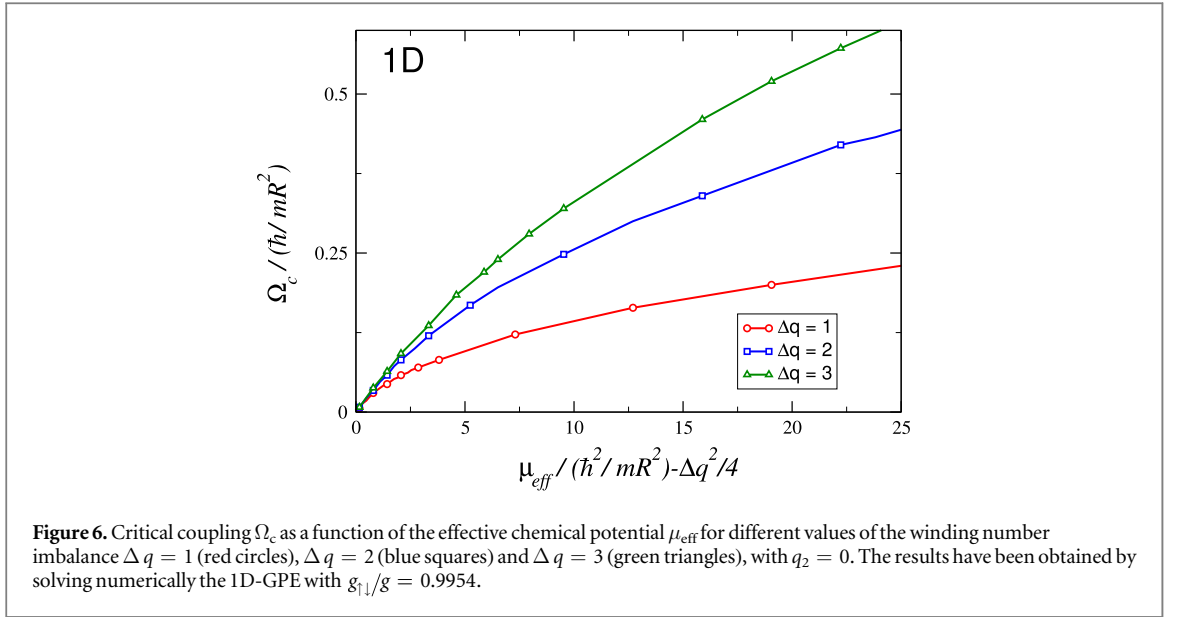
section we present the performance of CQPS in the case where the winding numbers imprinted onto both wavefunctions differ in more than one unit.

We have shown that in order to change the winding number in one unit, a $2\pi$-phase slip event involving the formation of an azimuthal density node has to occur. Therefore, to drive each component from winding number $q_1$ to $q_2$ (and viceversa), multiple number of such nodes ($|q_1 - q_2|$) must appear simultaneously. Multiple $2\pi$-phase slip can not occur through a sequence of single $2\pi$-phase slip events, since other states with winding number different from $q_1$ and $q_2$ would contribute, as described by the ansatz (6). This fact can be seen in figure 5, where we compare the numerical results of the GPE (white isocontours at 4% of maximum density and colors for the phase), with the analytical prediction for the same density isocontour given by equation (10) (black line), assuming that the system is in the Thomas–Fermi limit and equation (3) applies, for the initial state $|q_1 = 1, \; q_2 = 0\rangle$ (panel (a)) and $|q_1 = 2, \; q_2 = 0\rangle$ (panel (b)). The agreement is again excellent.
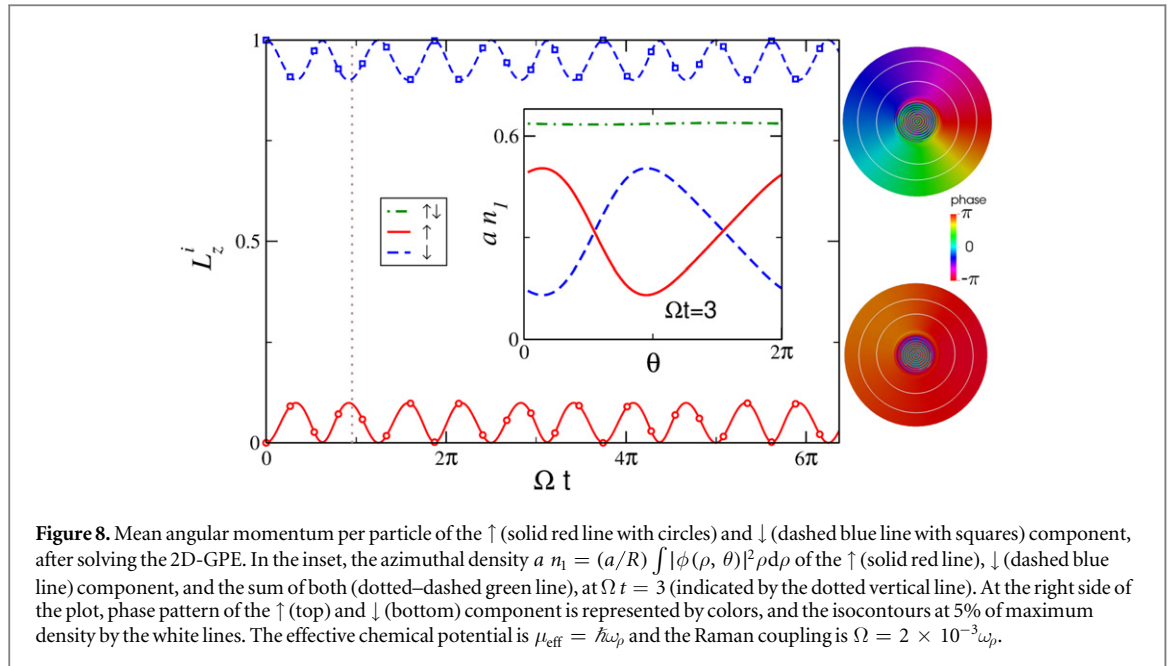
Figure 6 represents $\Omega_c$, which fixes the critical value of the Raman coupling that allows phase slip events, as a function of the effective chemical potential, for different initial winding number imbalances $\Delta q = 1, 2, 3$ (red circles, blue squares and green triangles, respectively), after solving the 1D-GPE with $g_{\uparrow\downarrow}/g = 0.9954$. $\Omega_c$ increases with $\mu_{\text{eff}}$, but this increasing is faster for larger initial $\Delta q$. The azimuthal nodes that the system has to generate in order to produce phase slips possess more energy, and the strength of the coherent coupling has to be larger to overcome higher energy barriers associated to smaller characteristic lengths.

We have studied the dynamics of the system for different initial winding number imbalance. Figure 7 shows the density (white isocontours) and the phase (color) of the ↑ component at a quarter of a Rabi cycle, for different values of the initial winding number $q_1$ (with $q_2 = 0$) imprinted onto condensates with $N = 5 \times 10^4$ atoms.

**Figure 6.** Critical coupling $\Omega_c$ as a function of the effective chemical potential $\mu_{eff}$ for different values of the winding number imbalance $\Delta q = 1$ (red circles), $\Delta q = 2$ (blue squares) and $\Delta q = 3$ (green triangles), with $q_2 = 0$. The results have been obtained by solving numerically the 1D-GPE with $g_{\uparrow\downarrow}/g = 0.9954$.



**Figure 7.** Density isocontours at 5% of maximum density and phase (color) of the $\uparrow$ component at a quarter of a Rabi cycle for a condensate of $N = 5 \times 10^4$ atoms, $\Omega = 200$ Hz and different values of the initial angular momentum imbalance, with the $\downarrow$ component first at rest. (a) $q_1 = 1$, (b) $q_1 = 2$, (c) $q_1 = 3$, (d) $q_1 = 4$, (e) $q_1 = 5$, (f) $q_1 = 6$, (g) $q_1 = 8$, (h) $q_1 = 10$ and (i) $q_1 = 16$. Only the cases of the first row do exhibit CQPS.

One can observe that density nodes appear equispaced forming an ordered pattern. As the initial angular momentum imbalance increases, the characteristic length scale associated to the azimuthal density nodes decreases as predicted by equation (10), and becomes closer to that of solitary waves as dark solitons or solitonic vortices. To generate such objects additional winding number modes have to be excited, and therefore, the CQPS process decays after few cycles. Then, the ansatz (6) is no longer valid. That is why the cases (c)–(i) of figure 7 will not exhibit CQPS (they belong to the NCQPS regime), and only the cases (a) and (b) will display this phenomenon. Each solitonic vortex that mediates the phase slip in the cases falling in the NCQPS regime contributes to the total mean angular momentum of each component according to equation (4).
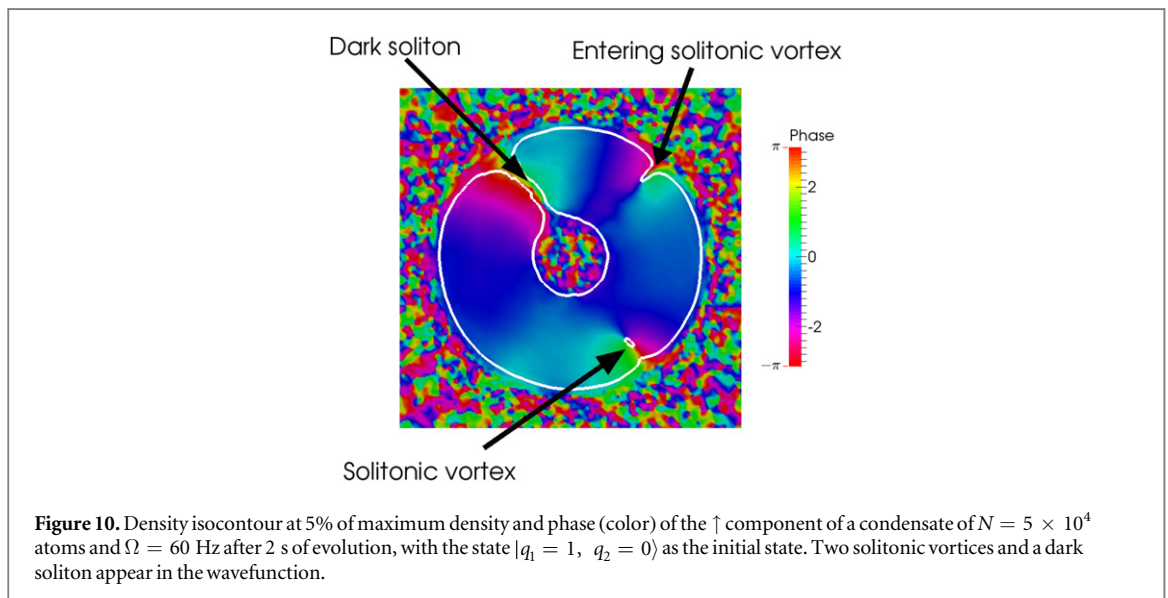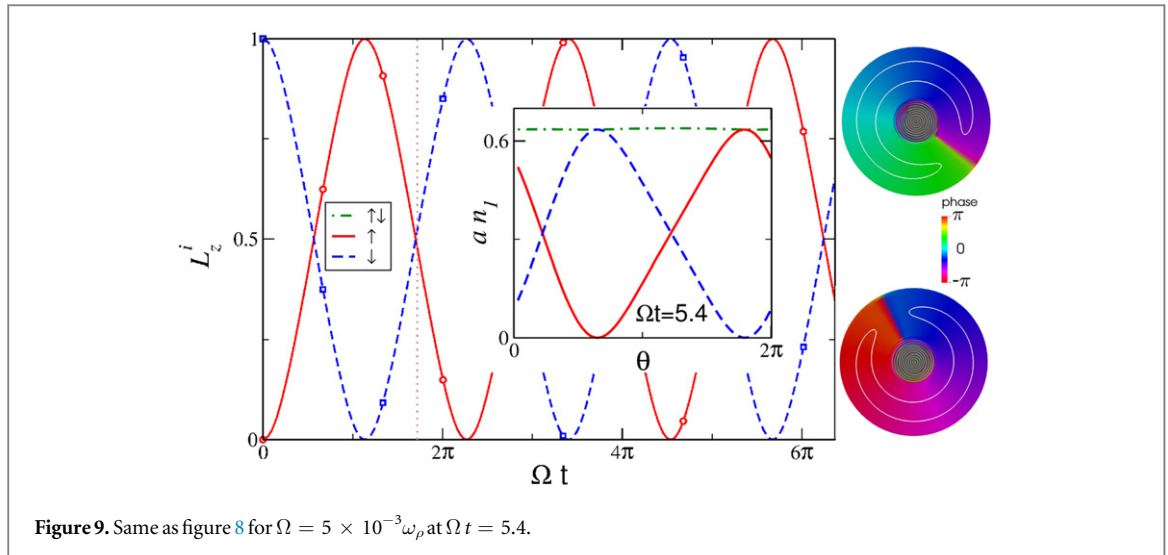
**Figure 8.** Mean angular momentum per particle of the ↑ (solid red line with circles) and ↓ (dashed blue line with squares) component, after solving the 2D-GPE. In the inset, the azimuthal density $a\, n_1 = (a/R) \int |\phi(\rho, \theta)|^2 \rho \, d\rho$ of the ↑ (solid red line), ↓ (dashed blue line) component, and the sum of both (dotted–dashed green line), at $\Omega\, t = 3$ (indicated by the dotted vertical line). At the right side of the plot, phase pattern of the ↑ (top) and ↓ (bottom) component is represented by colors, and the isocontours at 5% of maximum density by the white lines. The effective chemical potential is $\mu_{\text{eff}} = \hbar\omega_\rho$ and the Raman coupling is $\Omega = 2 \times 10^{-3}\omega_\rho$.

## 5. Other dynamical regimes

As was shown in figure 1, CQPS can not be found in the whole parameter space of the system, given that $g \neq g_{\uparrow\downarrow}$. Our numerical results point to the fact that CQPS exists as far as the ansatz (6) is valid, and this occurs for high values of the coherent coupling in comparison with $\Omega_c$. Below this critical value, we have found a dynamical regime where there is no vortex exchange between spin components. This fact is due to the presence of an energy barrier between winding number states $|q_1, q_2\rangle$ and $|q_2, q_1\rangle$, that prevents phase slips. Although such a barrier is of nonlinear nature, contrary to scalar condensates, it is not due to the existence of solitonic states on the total density of the system [25]. As mentioned before, the excitation of spin modes has been demonstrated to play a key role in spinor condensates coupled by density, and seems to be also relevant in this case. Such excitations are separated from the winding number states by the energy gap given in equation (5), which must be overcome in order to produce phase slips. If this critical energy can not be transferred between components by the coherent coupling, vortices will be trapped, and the mean angular momentum per component will not oscillate around the value $(q_1 + q_2)/2$.

Figure 8 shows a typical case representative of the trapping regime. It corresponds to the point A indicated in figure 1, for the coupling $\Omega = 2 \times 10^{-3}\omega_\rho$. As can be seen, the mean angular momentum of each component oscillates near the initial value, and the corresponding densities (shown in the inset after integration along the transverse section of the torus) present variations without nodal points. Although the interaction between components translate into currents inside each component (see the phase maps on the right of the figure), they are not enough to drive phase slips. Finally it is worth to note, that during all the time evolution the total density remains approximately constant along the torus.

When the Raman coupling takes intermediate values, $\Omega \gtrsim \Omega_c$, stable CQPS will not manifest in the dynamics, and the system enters the NCQPS regime. In this case, the coherent coupling is large enough to produce phase slip events that exchange the winding number between spin components. However, the time frequency of these events is lower than $\Omega$. This features are reflected in the case displayed in figure 9, corresponding to the point B of figure 1. Now the spin densities can show nodal points leading to phase slips, whereas the total density remains again approximately constant, although a small oscillation is present. As a consequence, and in contrast to the CQPS regime, the position of such nodal points for both components are not located at diametrically opposed positions. As the coherent coupling strength increases the frequency for phase slips approaches to $\Omega$.

In addition, as the chemical potential increases, the excitation of solitary waves (see panels (d)–(i) in figure 7) are responsible for the damping of the exchange of angular momentum between components. As a consequence, the system can deviate from the quasi-stationary path and explore other regions of the phase space. Different topological objects are generated, and then, the long-time dynamics will bring the condensate to an out-of-equilibrium quantum gas. Notice that in this regime many angular momentum modes are excited and the two-mode approach (6) is no longer valid. In figure 10 we show a characteristic snapshot of the density and the phase of the ↑ component of a condensate with $N = 5 \times 10^4$ atoms and Raman coupling $\Omega = 60$ Hz after 2 s of evolution from the initial state $|q_1 = 1, q_2 = 0\rangle$. The white line traces the density isocontour at 5% of

**Figure 9.** Same as figure 8 for $\Omega = 5 \times 10^{-3}\omega_\rho$ at $\Omega t = 5.4$.



**Figure 10.** Density isocontour at 5% of maximum density and phase (color) of the ↑ component of a condensate of $N = 5 \times 10^4$ atoms and $\Omega = 60$ Hz after 2 s of evolution, with the state $|q_1 = 1, \; q_2 = 0\rangle$ as the initial state. Two solitonic vortices and a dark soliton appear in the wavefunction.

maximum density and the colors display the phase. In the figure one can also see that although the initial angular momentum imbalance is $\Delta q = 1$, several kinds of solitary waves (a dark soliton and two solitonic vortices) are excited in the condensate in order to try to drive a single $2\pi$-phase slip. One can see that the appearance of solitonic vortices do not accomplish with the azimuthal dependence of the density predicted by equation (10), and as a consequence, it is not compatible with CQPS.

## 6. Summary and conclusions

In the present work we have proposed an atomic analogue of the Mooij–Harmans qubit that displays CQPS. Two-component condensates loaded on toroidal atomtronic circuits can display phase slips by virtue of the coherent coupling. When a vortex pattern phase is imprinted onto each component with different winding number, the system evolves through quasi-stationary states that are a superposition of both winding number states. The two components exchange vortices by phase slip events modulated by the coupling, in such a way that the mean angular momentum imbalance oscillates with the Raman frequency.

　　We have identified the different dynamical regimes of the system as a function of the coherent coupling and the effective chemical potential. In particular, we have focused on the dynamical phase corresponding to CQPS, where the system behaves effectively as linear despite the nonlinearity. For this regime, we have mapped the dynamics of the coupled system onto linear Josephson equations by using an ansatz composed of two winding number modes per component. The whole dynamics, and specifically the results obtained for the mean angular momentum imbalance and the density, are very accurately reproduced by our analytical model. This model

predicts that CQPS needs phase slip events to occur through azimuthal density nodes, otherwise coherence would be destroyed. Our numerical results obtained by solving the time-dependent GPE confirm these predictions.

We would like to point out the experimental feasibility of this system, since we have used values for the physical parameters currently available in laboratories. $^{87}$Rb is a good candidate to perform this qubit, mainly, for the closeness of the scattering lengths. Toroidal condensates that have been recently obtained have a diameter of the order of 10–20 $\mu$m, while ours is 15 $\mu$m. The Raman coupling does not present any strong limitation for its value although commonly, it ranges from a few Hz, to kHz hundreds. Besides, phase imprinting techniques have improved in the last decade and the individual manipulation of a single component of a spinor BEC is possible nowadays.

The qubit we have proposed points to multiple possibilities in the field of cold atoms. The control of the coherent coupling permits to freeze the system in quasi-stationary persistent current states with non-quantized angular momentum characteristic of linear superposition of quantum states. Since both current states are entangled, one can manipulate the quantum superposition of both flow states, performing as a good quantum computer gate, and offering paths for improvements in quantum information processing. The theoretical analysis discussing the role of nonlinear objects, as relative phase domain walls and dark solitons, are out of the scope of the present article and will be addressed in the future.

## Acknowledgments

## References

[1] Jaklevic R C, Lambe J, Silver A H and Mercereau J E 1964 *Phys. Rev. Lett.* **12** 159
[2] Jaklevic R C, Lambe J, Mercereau J E and Silver A H 1965 *Phys. Rev.* **140** A1628
[3] Anderson M H, Ensher J R, Matthews M R, Wieman C E and Cornell E A 1995 *Science* **269** 198
[4] Davis K B, Mewes M O, Andrews M R, van Druten N J, Durfee D S, Kurn D M and Ketterle W 1995 *Phys. Rev. Lett.* **75** 3969
[5] Seaman B T, Krämer M, Anderson D Z and Holland M J 2007 *Phys. Rev. A* **75** 023615
[6] Ryu C, Andersen M F, Cladé P, Natarajan V, Helmerson K and Phillips W D 2007 *Phys. Rev. Lett.* **99** 260401
[7] Moulder S, Beattie S, Smith R P, Tammuz N and Hadzibabic Z 2012 *Phys. Rev. A* **86** 013629
[8] Wright K C, Blakestad R B, Lobb C J, Phillips W D and Campbell G K 2013 *Phys. Rev Lett.* **110** 025302
[9] Ryu C, Blackburn P W, Blinova A A and Boshier M G 2013 *Phys. Rev. Lett.* **111** 205301
[10] Eckel S, Lee J G, Jendrzejewski F, Murray N, Clark C W, Lobb C J, Phillips W D, Edwards M and Campbell G K 2014 *Nature* **506** 200
[11] Albiez M, Gati R, Fölling J, Hunsmann S, Cristiani M and Oberthaler M K 2005 *Phys. Rev. Lett.* **95** 010402
[12] Levy S, Lahoud E, Shomroni I and Steinhauer J 2007 *Nature* **449** 579
[13] Sols F 1999 Josephson effect between Bose condensates *Bose–Einstein Condensation in Atomic Gases, Proc. Int. School of Physics 'Enrico Fermi'* ed M Inguscio *et al* (Amsterdam: IOS Press)
[14] Williams J E, Walser R, Cooper J, Cornell E A and Holland M J 1999 *Phys. Rev. A* **59** R31(R)
[15] Matthews M R, Anderson B P, Haljan P C, Hall D S, Wieman C E and Cornell E A 1999 *Phys. Rev. Lett.* **83** 2498
[16] Williams J E and Holland M J 1999 *Nature* **401** 568
[17] Anderson P W 1966 *Rev. Mod. Phys.* **38** 298
[18] Arutyunov K Y, Golubev D S and Zaikin A D 2008 *Phys. Rep.* **464** 1
[19] Varoquaux E 2015 *Rev. Mod. Phys.* **87** 803
[20] Langer J S and Ambegaokar V 1967 *Phys. Rev.* **164** 498
[21] Piazza F, Collins L A and Smerzi A 2009 *Phys. Rev. A* **80** 021601(R)
[22] Piazza F, Collins L A and Smerzi A 2013 *J. Phys. B: At. Mol. Opt. Phys.* **46** 095302
[23] Abad M, Guilleumas M, Mayol R, Pi M and Jezek D M 2011 *Phys. Rev. A* **84** 035601
[24] Abad M, Guilleumas M, Mayol R, Piazza F, Jezek D M and Smerzi A 2015 *Europhys. Lett.* **109** 40005
[25] Muñoz Mateo A, Gallemí A, Guilleumas M and Mayol R 2015 *Phys. Rev. A* **91** 063625
[26] Leggett A J and Garg A 1985 *Phys. Rev. Lett.* **54** 857
[27] Schenke C, Minguzzi A and Hekking F 2011 *Phys. Rev. A* **84** 053636
[28] Halkyard P L, Jones M P A and Gardiner S A 2010 *Phys. Rev. A* **81** 061602(R)
[29] Amico L, Osterloh A and Cataliotti F 2005 *Phys. Rev. Lett.* **95** 063201
[30] Amico L, Aghamalyan D, Auksztol F, Crepaz H, Dumke R and Kwek L C 2014 *Sci. Rep.* **4** 4298
[31] Aghamalyan D, Amico L and Kwek L C 2013 *Phys. Rev. A* **88** 063627
[32] Aghamalyan D, Cominotti M, Rizzi M, Rossini D, Hekking F, Minguzzi A, Kwek L C and Amico L 2015 *New J. Phys.* **17** 045023
[33] Hallwood D W, Ernst T and Brand J 2010 *Phys. Rev. A* **82** 063623
[34] Hallwood D W and Brand J 2011 *Phys. Rev. A* **84** 043620
[35] Gallemí A, Guilleumas M, Martorell J, Mayol R, Polls A and Juliá-Díaz B 2015 *New J. Phys.* **17** 073014
[36] Astafiev O V, Ioffe L B, Kafanov S, Pashkin Y A, Arutyunov K Y, Shahar D, Cohen O and Tsai J S 2012 *Nature* **484** 355
[37] Mooij J E and Harmans C J P M 2005 *New J. Phys.* **7** 219
[38] Mooij J E and Nazarov Y V 2006 *Nat. Phys.* **2** 169
[39] Lim J, Lee H G, Lee S, Park C Y and Ahn J 2014 *Sci. Rep.* **4** 5867

[40] Ho T L and Shenoy V B 1996 *Phys. Rev. Lett.* **77** 3276

[41] Riboli F and Modugno M 2002 *Phys. Rev.* A **65** 063614

[42] Polo J, Mason P, Sridhar S, Billam T P, Ahufinger V and Gardiner S A 2015 *Phys. Rev.* A **91** 053626

[43] Brand J, Haigh T J and Zülike U 2010 *Phys. Rev.* A **81** 025602

[44] Guilleumas M and Graham R 2001 *Phys. Rev.* A **64** 033607

[45] Pethick C J and Smith H 2002 *Bose–Einstein Condensation in Dilute Gases* (Cambridge: Cambridge University Press)

[46] Leggett A J 1999 *AIP Conf. Proc.* **477** 154

[47] Son D T and Stephanov M A 2002 *Phys. Rev.* A **65** 063621

[48] Abad M and Recati A 2013 *Eur. Phys. J.* D **67** 148

[49] García-Ripoll J J, Pérez-García V M and Sols F 2002 *Phys. Rev.* A **66** 021602(R)

[50] Williams J E 1999 The preparation of topological modes in a strongly coupled two-component Bose–Einstein condensate *PhD Thesis* University of Colorado

[51] Dum R, Cirac J I, Lewenstein M and Zoller P 1998 *Phys. Rev. Lett.* **80** 2972